



**HAL**  
open science

## Cluster versus ROI analysis to assess combined antiangiogenic therapy and radiotherapy in the F98 rat-glioma model

Nicolas Coquery, Raphaël Serduc, Chantal Rémy, Emmanuel Luc Barbier, Benjamin Lemasson

### ► To cite this version:

Nicolas Coquery, Raphaël Serduc, Chantal Rémy, Emmanuel Luc Barbier, Benjamin Lemasson. Cluster versus ROI analysis to assess combined antiangiogenic therapy and radiotherapy in the F98 rat-glioma model. *NMR in Biomedicine*, 2018, 31 (8), pp.e3933. 10.1002/nbm.3933 . hal-01808105

**HAL Id: hal-01808105**

**<https://univ-rennes.hal.science/hal-01808105>**

Submitted on 3 Sep 2018

**HAL** is a multi-disciplinary open access archive for the deposit and dissemination of scientific research documents, whether they are published or not. The documents may come from teaching and research institutions in France or abroad, or from public or private research centers.

L'archive ouverte pluridisciplinaire **HAL**, est destinée au dépôt et à la diffusion de documents scientifiques de niveau recherche, publiés ou non, émanant des établissements d'enseignement et de recherche français ou étrangers, des laboratoires publics ou privés.

## **Title Page**

### ***Title:***

**Cluster versus ROI analysis to assess combined antiangiogenic and radiotherapy in F98 rat-glioma model**

***Short title:*** MRI-based clustering to monitor combined therapies in glioma

### ***Author affiliation:***

Nicolas Coquery<sup>1,2,3</sup>, Raphael Serduc<sup>4</sup>, Chantal Rémy<sup>1,2</sup>, Emmanuel Luc Barbier<sup>1,2\*</sup> and Benjamin Lemasson<sup>1,2</sup>

<sup>1</sup>Univ. Grenoble Alpes, Grenoble Institut des Neurosciences, GIN, F-38000 Grenoble, France

<sup>2</sup>Inserm, U1216, F-38000 Grenoble, France

<sup>3</sup>INRA, INSERM, Univ Rennes, Nutrition Metabolisms and Cancer, NuMeCan, 35000 Rennes, France

<sup>4</sup>Rayonnement synchrotron et Recherche médicale, Université Grenoble Alpes, EA 7442, 71 rue des Martyrs, 38000 Grenoble, France

### ***\*Corresponding author:***

Emmanuel L. BARBIER

U1216 – Grenoble Institut des Neurosciences

Chemin Fortuné Ferrini

38700 La Tronche

France

Tel: +33 4 56 52 05 88 / Fax: +33 4 56 52 05 98

E-Mail: [emmanuel.barbier@univ-grenoble.alpes.fr](mailto:emmanuel.barbier@univ-grenoble.alpes.fr)

***Words Count:*** 4817

## **Abstract**

For glioblastoma (GBM), current therapeutic approaches focus on the combination of several therapies, each of them individually approved for GBM or other tumor types. Many efforts are made to decipher the best sequence of treatments that would ultimately promote the most efficient tumor response. There is therefore a strong interest in developing new clinical *in vivo* imaging procedures that can rapidly detect treatment efficacy and allow individual modulation of the treatment. In this preclinical study, we propose to evaluate tumor tissue changes under combined therapies, tumor vascular normalization under antiangiogenic treatment followed by radiotherapy, using a voxel-based clustering approach. This approach was applied to a rat model of glioma (F98). Six MRI parameters were mapped: apparent diffusion coefficient, vessel wall permeability, cerebral blood volume fraction, cerebral blood flow, tissue oxygen saturation and vessel size index. We compared the classical region of interest (ROI)-based analysis with a cluster-based analysis. Five clusters, defined by their MRI features, were sufficient to characterize tumor progression and tumor changes during treatments. These results suggest that the cluster-based analysis was as efficient as the ROI-based analysis to assess tumor physiological changes during treatment but also gave additional information regarding the voxels impacted by treatments and their localization within the tumor. Overall, the cluster-based analysis appears as a powerful tool for subtle monitoring of tumor changes during combined therapies.

## **Keywords:**

MRI, unsupervised clustering, radiomics, brain, glioma, combined therapies.

***Abbreviations:***

ADC: apparent diffusion coefficient

CBF: Cerebral blood flow

CBV: cerebral blood volume

GBM: glioblastoma

Perm: vascular wall integrity

ROI: region of interest

StO<sub>2</sub>: tissue saturation in oxygen

VSI: vessel size imaging

# 1. Introduction

Among the strong efforts to develop new therapies against glioma, current strategies combine several therapies in order to cumulate their effects and ultimately reach a synergic efficiency. This was initially applied in the Stupp's *et al.*<sup>1</sup> protocol in which resection, chemotherapy and radiotherapy are combined. Since the routine application of this protocol in clinic, other combined therapeutic approaches became relevant in glioma management<sup>2,3</sup>, and complex combinations of antiangiogenic therapy, chemotherapy and radiotherapy underwent clinical trials<sup>4,5</sup>. Depending on the therapy and its biological target, the sequence of treatments remains a central question. As example, Jain suggested that an antiangiogenic-based vascular normalization<sup>6</sup> could increase the effects of concurrent radiotherapy<sup>7</sup>.

In this context, there is an obvious need for consistent tumor monitoring methods such as multiparametric MRI in order to rapidly assess the efficacy of complex combined therapies. Indeed, MRI gives access to many parameters (i.e. water diffusion, blood volume and blood flow<sup>8</sup>, microvessel size and density<sup>9</sup>, local blood oxygen saturation<sup>10</sup>, vessel wall permeability<sup>11</sup>, vessel vasoreactivity<sup>12</sup>). Recently, Lemasson et al. have shown that multiparametric MRI can monitor the effects of individual therapies (antiangiogenic and radiotherapy), used concomitantly, on a 9L glioma model<sup>13</sup>. This study used the classical region of interest (ROI)-based MRI analysis, an approach with 2 major limitations: i) it gives an averaged view of the tumor response and therefore it does not take into account the intra-tumoral heterogeneity and ii) it does not exploit the full potential of the multiparametric MR protocol (one voxel contains multiple information). Alternatively, voxel-based analysis of tumor progression and response to treatments seems to be more suited for this purpose<sup>14</sup> but this method is often limited to a single MRI parameter. In order to overcome these limitations, we recently proposed an unsupervised clustering method based on probabilistic mixture models<sup>15</sup> yielding histological-like maps that can potentially integrate a broad range of MRI

parameters<sup>16</sup>. This multiparametric MRI-based approach coupled with unsupervised clustering might be well suited to decipher the complex information measured during combined therapies on brain tumors.

In the context of combined cancer therapies (antiangiogenic therapy followed by radiotherapy), we compare in this study the data generated by the classical ROI-based analysis (parameter by parameter) and a cluster-based analysis of six MRI parameters. MRI parameters were measured on well-established F98 tumors in rats during tumor growth under single antiangiogenic or radiotherapy treatment and under combined therapies. The ROI-based analysis was able to highlight the averaged tumor changes while the cluster-based analysis yielded additional information about tumor regions that respond to treatment.

## 2. Experimental details

The study design was approved by the local institutional animal care and use committee (COMETHS). All animal procedures conformed to French government guidelines and were performed under permits 380820 and B3851610008 (for experimental and animal care facilities) from the French Ministry of Agriculture. This study is in compliance with the ARRIVE guidelines (Animal Research: Reporting in Vivo Experiments<sup>17</sup>). All procedures were performed under isoflurane anesthesia (5% for induction and 2.5% for maintenance). The tail vein was equipped with a catheter when needed. The rectal temperature was monitored and maintained at 37.0°C.

**2.1 Animal Model.** The F98 cells ( $10^3$  cells, ATCC: CRL-2397) were implanted in the right caudate nucleus of male Fischer 344 rats (n=19, 7 weeks, 175-200 g, Charles River, France) with a stereotactic frame, as previously described<sup>18</sup>.

**2.2 In vivo experiment.** The experimental design is presented Fig 1, with D as notation for the duration (days) after tumor cell implantation, and T as the duration (days) after treatment initiation. The different treatment groups are described in the figure legend. *Antiangiogenic treatment:* Sorafenib (Sora: 30 mg/kg in vehicle, Bayer Biosciences) or vehicle (DMSO: 5%, Tween20: 5%, NaCl0.9%: 90%) were administered p.o. (approximately 1mL) every day during three days (D21T0 to D23T2). *Radiotherapy:* animals received in one session, at D24T3, 20Gy directed into the tumor ipsilateral hemisphere (GenX, ESRF). Conventional orthovoltage irradiations were performed using a Philips X-ray generator operated at 200 kVp. A dose rate of 1.61 Gy/min was delivered at the centre of the intracerebral tumor using an ionization chamber (Semiflex 31010, PTW). *Imaging:* Three MRI sessions were performed

at 4.7 T (Avance III console; Bruker, Ettlingen, Germany; IRMaGe MRI facility, Grenoble, France) between 20 and 26 days after tumor implantation (D20T-1, D24T3 and D26T5).

**2.3 MRI session.** The following imaging sequences were performed with a voxel size of  $234 \times 234 \times 800 \mu\text{m}$  unless stated otherwise. *Anatomical imaging* was performed with a T<sub>2</sub>-weighted (T<sub>2</sub>W) spin-echo sequence to determine tumor volume. The *apparent diffusion coefficient (ADC)* was mapped using a spin-echo EPI sequence (3 orthogonal diffusion directions,  $b \approx 0$  and  $b = 900 \text{ s/mm}^2$ ). *Cerebral blood flow (CBF)* was determined using pseudo continuous arterial spin labelling (pCASL) with an EPI readout (labelling duration=3s, post-labelling delay=400 ms, 50 pairs)<sup>19</sup> and a T<sub>1</sub> map. To map the *tissue saturation in oxygen (StO<sub>2</sub>)*, a T<sub>2</sub> map (28 spin echoes between 12 and 336 ms) and a high resolution T<sub>2</sub>\* map (25 gradient echoes between 3 and 87 ms; voxel size=  $117 \times 117 \times 200 \mu\text{m}$ ) were obtained. A *cerebral blood volume (CBV)* and a *vessel size imaging (VSI)* maps were obtained using a steady-state approach<sup>20</sup> and ultrasmall superparamagnetic iron oxide nanoparticles (P904: 200  $\mu\text{moles}$  of iron/kg body weight; Guerbet SA, France). *The vascular wall integrity (Perm)* was assessed using a dynamic contrast-enhanced MRI approach as previously described<sup>21</sup>. Briefly, 25 T<sub>1</sub>-weighted, spin-echo, images were acquired. After acquisition of 4 baseline images, a bolus of Gd-DOTA (200  $\mu\text{mol/kg}$ ; Guerbet SA, France) was administered through the tail vein. The image acquisition positions were identical for all quantitative MRI sequences.

**2.4 Data processing.** Image processing was performed within the Matlab 7 environment (The MathWorks Inc., Natick, MA, USA) using custom software. The *CBF* computation was based on the equations described in Alsop et al.<sup>22,23</sup>. The *VSI* and *CBV* were derived from the transverse relaxivities as described<sup>20</sup>. *StO<sub>2</sub>* maps were estimated using a multiparametric

qBOLD approach as previously described<sup>24-26</sup>. *Perm* was estimated by calculating the area under the signal enhancement curve following the Gd-DOTA injection (between images 5 and 14, which corresponds to 150 sec), after baseline removal<sup>21</sup>.

**2.5 Data analysis.** To determine the tumor volume, tumor ROIs were manually delineated on the T<sub>2</sub>W images that covered the entire brain. For tumor delineation, all visible abnormalities (hyper- and hypo-intense signals) were included. Parameter values were obtained using the same tumor ROIs and the five shared MRI slices between all sequences.

Two type of measurements were performed:

- A ROI selection followed by an analysis of the mean ROI values. Voxels were included in the analysis according to the following criteria:  $0 < \text{ADC} < 2500 \mu\text{m}^2/\text{s}$  (percentage of included voxels=97.9%),  $\text{Perm} < 2.5 \times 10^6 \text{ a.u.}$  (percentage of included voxels=99.3%),  $0 < \text{CBF} < 400 \text{ mL}/100\text{g}/\text{min}$  (percentage of included voxels=83.0%),  $0 < \text{CBV} < 20 \%$  (percentage of included voxels=96.8%),  $0 < \text{VSI} < 50 \mu\text{m}$  (percentage of included voxels=82.6%) and  $0 < \text{StO}_2 < 100\%$  (percentage of included voxels=53.2%). Beyond these ranges, values cannot be considered physiologically accurate. Average values were computed across all animals for each ROI and each parameter (Fig 2A).
- The ROI selection as above followed by a model-based clustering<sup>15</sup> analysis. For each MR parameter, values were standardized to minimize scale effects between parameters using the following formula:  $(\text{voxel value} - \text{mean across all voxels}) / \text{standard deviation across all voxels}$ . In order to avoid exclusion of voxels with non-physiological value in only one map, we included all values for each map that were comprised between the first and the last percentile of the distributed values (percentage of included voxels=90,6%). All included voxels of all animals were pooled together and analysed with an unsupervised

clustering method based on mixture of Gaussian models, as previously described<sup>16</sup>. Briefly, Gaussian mixture modelling was performed using the Expectation–Maximization algorithm implemented in the R package mclust<sup>15</sup>. The optimal number of clusters was determined using a Bayesian information criterion and was estimated to 5 clusters. For this analysis, two rats belonging to the V and VRT groups were excluded due to computation problems in at least one MRI parameter.

**2.6 Statistical analysis.** Repeated measures-ANOVA (RM-ANOVA) was used to evaluate the change of each parameter between imaging sessions. In case more than two groups were analysed, a LSD post-hoc was used. Mann-Whitney test was used to evaluate the effects of treatments on change in MRI parameters and in cluster-ratio. A  $p$ -value  $< 0.05$  was considered significant.

### 3. Results

**3.1 ROI-based evaluation of Sorafenib and radiotherapy effects considering all data and time points (Fig 2A).** The consequence of the ROI-based evaluation is the loss of spatial information within tumor that leads to an averaged representation of each parameter for the studied ROIs as schematically represented in Fig 2B. However, the comparison between mean ROI values shows the effects of the different treatments at different time-points (Fig 2C) while mean tumor size does not change, whatever the treatment applied (Fig 2D). In order to limit the impact of tumor volume on voxels clustering, the average tumor size was similar between groups before treatment (D20T-1; group V:  $133.9 \pm 46.4 \text{mm}^3$ , group S:  $116.7 \pm 48.9 \text{mm}^3$ ). Between D20T-1 and D24T3, Sora treatment (group S) promotes a significant decrease in vessel wall permeability, a stabilization of the CBF compared with untreated tumors (group V, Fig 2C) and a tendency towards increased apparent diffusion coefficient (ADC,  $p=0.084$ ). Between D24T3 and D26T5, the effects of concomitant radiotherapy could not be extensively characterized by the ROI-based analysis. Indeed, we only observed a significant decrease in CBF between D24T3 and D26T5 after Sora treatment (group S $\emptyset$ ) and after Sora treatment followed by the radiation therapy (group SRT), compared with vehicle administration followed by the radiation therapy (group VRT).

**3.2 Clustering-based evaluation for tumor follow-up and characterization of treatment effects.** To assess the effects of treatments on tumors, we used an unsupervised, model-based clustering analysis, which integrates the 6 quantitative MRI parameters (ADC, Perm, CBF, CBV, VSI and StO<sub>2</sub>) and identifies clusters of voxels sharing the same MRI physiological characteristics. This analysis was performed on voxels from the previously defined tumor ROIs; the voxels from all time points and under all treatments were pooled.

The characterization of clusters with standardized MRI parameters values (Fig 3A, web graphs) and raw values allows discriminating the signature of one cluster from that of other clusters:

- cluster *a* presents the highest levels of CBF, CBV, StO<sub>2</sub> and the lowest levels of VSI, ADC and Perm (20.5% of voxels belong to cluster *a*).
- cluster *b* is characterized by the highest levels of Perm and VSI, a high level of CBV, a reduced level of StO<sub>2</sub> and an intermediate level of CBF and ADC (19.6% of voxels belong to cluster *b*).
- cluster *c* is the less represented cluster (only 9.5% of voxels belong to cluster *c*). Compared to cluster *a* and *b*, the levels of CBV and CBF are reduced and the levels of Perm and ADC are increased.
- cluster *d* is similar to cluster *c* with reduced parameters values (26.7% of voxels belong to cluster *d*).
- cluster *e* has the highest level of ADC with a high level of VSI and the lowest levels of CBF and CBV (14.4% of voxels belong to cluster *e*).

From cluster *c* to *e*, the levels of Perm and CBV gradually decrease and the level of StO<sub>2</sub> meets non-physiological value (too low perfusion). When taking into account the voxels within the three time points and the different treatments, a visual inspection of the cluster distributions (Fig 3B) shows spatially coherent patterns of voxels belonging to a same cluster. Whatever the time points and treatments, cluster *a* (purple) is mainly located at the tumor margins, cluster *c* (yellow) distribution is sparse and cluster *d* (grey) proportion is stable and found as groups of numerous neighbouring voxels.

The RM-ANOVA-based statistical analysis of the proportions of each cluster in the tumor between treatments and time points does not yield consistent information (Fig 3B, coloured bar graphs). However, the bar graphs on Fig 3B show that cluster *b* (green) proportion

decreases for all treatment conditions (Sora treatment: V vs S at D24T3; radiotherapy: V at D24T3 vs VRT at D26T5 for the same tumor). Cluster *e* (red), rarely found at the earliest time point (D20T-1), increases in proportion after treatment.

### 3.3 Spatial detection of treatments effects

Tumor properties and associated MR parameters depend on (i) the tumor growth, (ii) the type of treatment and (iii) the specific sequence of Sorafenib and radiotherapy treatments. In order to investigate the effects of each treatment, we choose to analyse the changes between two time points using 2 approaches: (i) the ROI-based MRI parameters values, determined as the change (in percentage) of each parameter value and (ii) the cluster proportion within ROI, determined as the change (in percentage) in the number of voxels per cluster (Fig 4). This approach allowed the description of the effect of each treatment for a given time interval whatever tumor growth and the type of treatment given in the previous time interval.

#### 3.4.1 Between D20T-1 and D24T3, Sorafenib effects (Fig 4A and C).

Using the ROI-based changes in MRI parameters, we measured increased levels of ADC ( $+4.1\pm 1.7\%$ ), Perm ( $+17.0\pm 21.4\%$ ) and VSI ( $+15.8\pm 9.9\%$ ) and decreased levels of CBF ( $-32.3\pm 6.7\%$ ), CBV ( $-13.7\pm 5.9\%$ ) and StO<sub>2</sub> ( $-10.0\pm 3.5\%$ ) during tumor growth under vehicle administration (Fig 4A, group V). Compared with vehicle administration, Sorafenib treatment significantly increased the level of CBF ( $+5.2\pm 16.3\%$ ,  $p=0.018$ ), reinforced the increase in ADC ( $+10.0\pm 2.9\%$ ,  $p=0.028$ ) and oppositely decreased the Perm ( $-31.4\pm 10.3\%$ ,  $p=0.011$ ). These variations are in good agreement with the antiangiogenic effects of Sorafenib.

Using the cluster-based change approach, during tumor growth under vehicle administration (Fig 4C, group V), we measured a decreased proportion of cluster *a* ( $-14.5\pm 5.5\%$ ), and increased proportions of all other clusters (*b*:  $+3.8\pm 2.5\%$ , *c*:  $+4.3\pm 4.9\%$ , *d*:  $+1.1\pm 3.3\%$ , *e*:

+4.5±1.4%). Compared with vehicle administration, Sorafenib treatment maintained the proportion of cluster *a* stable (-1.5±2.4%, p=0.035) and decreased the proportion of cluster *b* (-11.0±3.0%, p=0.006).

#### 3.4.2 Between D24T3 and D26T5, radiotherapy or combined treatments effects (Fig 4B and D).

The approach of ROI-based changes (Fig 4B) showed an increased level of ADC after radiotherapy alone or in combination with Sorafenib treatment as compared to the Sorafenib treatment alone (VRT=+9.9±1.6%, p=0.042 and SRT=+6.7±2.4%, p=0.088 versus SØ=-0.5±3.6%). The effect of radiotherapy after Sorafenib treatment (SRT) was detected as a significant change of CBV (VRT=-19.3±2.3% vs SRT=-6.8±3.8%, p=0.018). Radiotherapy alone promoted a decrease of CBV similar to the decrease measured in the SØ group, whereas SRT treatment maintained a level of CBV similar to an estimated control value (vehicle without radiotherapy: VØ) determined as the change in parameter between D20T-1 vs D24T3 under vehicle administration and corrected for a two-days tumor growth (VRT=-19.3±2.3%, SRT=-6.8±3.8%, SØ=-21.0±13.3% and estimated VØ=-6.85%). Note that, two days after the end of Sorafenib administration (SØ), ADC, Perm and CBF, initially modified by Sorafenib, returned back to the estimated control values measured between D20T-1 and D24T3.

The cluster-based change approach (Fig 4D) revealed a significant decrease in the proportion of cluster *a* after Sorafenib administration as compared to radiotherapy alone (VRT=-5.3±2.3% vs SØ=-17.0±7.6%, p=0.028). Compared with the estimated control value between D24T3 and D26T5 (estimated VØ), cluster *b* proportion was also decreased after radiotherapy alone (VRT=-11.7±5.2% vs estimated VØ=1.9%, p=0.016).

The effects of combined treatments were detected as a lower increase in the proportion of cluster *e* when radiotherapy was applied after Sorafenib treatment compared with radiotherapy alone (SRT=+2.9±1.1% vs VRT=+9.3±4.2%, p=0.028). No difference between treatment conditions was detected for clusters *c* and *d*. The changes in the proportions of these clusters are similar for all treatment conditions and follow the tendency of the estimated control changes.

## 4. Discussion

This study presents a comparison of ROI-based and cluster-based analyses of MRI data collected during the follow-up of a rat glioma model under several therapeutic combinations, Sorafenib and/or radiotherapy. We developed a comprehensive analysis strategy in order to alleviate bias related to the effect of one therapy to the other and to the tumoral status before treatment. The ROI-based analysis appears well-suited to highlight global tumoral changes but filters out local changes whereas the cluster-based analysis appears as a powerful approach to detect voxel-based variations within the tumor that are impacted by (i) tumor growth, (ii) single or (iii) combined treatments.

Given that the ROI- and the cluster-based analyses are known to reflect biological features such as seen in histology<sup>16,27,28</sup>, we focused on the comparison of the ability of these two approaches to monitor the tumor changes under therapies. MRI data included six parameters (ADC, Perm, CBV, CBF, VSI and StO<sub>2</sub>) known to change during tumor development<sup>29–33</sup> and that may be additionally modulated by the anti-tumor therapies used in this study<sup>25,34,35</sup>.

The manually delineated tumor ROI contoured all the abnormalities observed on the T<sub>2</sub>W images, including oedema and peritumoral cell infiltration, and thereby maximized the number of different tissue types. This approach also permitted to minimize inter-rater variability between different delineated tumors and to include all putative abnormalities. With the clustering strategy, we did not observe the emergence of new tissue types during tumor progression or treatment with the cluster-based analysis (all clusters were present at all time points).

The effects of the different therapies were detected by the ROI-based analysis of some MRI parameters (ADC, Perm, CBV, and CBF). However, the visualization of the average values of these parameters within tumor bulk (Fig 2B) shows that this analysis filters out the spatial heterogeneity of tumor characteristics during progression and treatment and does not account

for joint changes in parameters (e.g. decreased CBF and increased Perm). Conversely, the cluster-based approach allows the integration of all MRI parameters in one synthetic map. A visual inspection of the resulting map shows that, without using any knowledge of the spatial or temporal organization of voxels, the present clustering yields spatially-structured and temporally-consistent maps of clusters. For instance, at D20T-1, voxels with high CBF value are localized at the tumor border and cluster *a*, which is mainly distributed at this localization, accordingly presents the highest CBF value. Over time, cluster *a* remains at the periphery of the tumor. Besides topological information, the cluster-based approach defines for each cluster a profile accounting for all MRI parameters and thereby discriminates homogenous groups of voxels within the tumor that cannot be detected by inspecting the ROI-based analysis. We observe that the variability of the change in cluster proportions during treatment is lower than that of the ROI-based parameter values (see the SEM in Figure 4). This lower variability may be ascribed to the fact that clusters represent homogeneous ranges of parameter values and thus a fraction of the tumor while ROI integrate the range of a parameter values across the entire tumor. This lower variability of the change in cluster proportions suggests that the cluster-based analysis is more sensitive to changes within the tumor than the ROI-based analysis. This can be illustrated by CBV or VSI, which may be reduced by Sorafenib treatment<sup>13,25</sup>: they were not detected as changed following Sorafenib treatment by the ROI-based analysis, whereas, the proportion of cluster *b*, which presents the highest levels of CBV and VSI, was reduced. Our results show that, when specific areas within a tumor respond to a therapy, the ROI-based analysis may be blind to these effects. Indeed, its global analysis erases all fine variations. This further suggests that the cluster-based approach might be less sensitive than ROI-based analysis to the inter-rater variability generally observed during tumor delineation. Indeed, we expect that the inter-rater variability will affect differently the ROI-based and the voxel-based analysis. The mean value

determined with the ROI-based analysis will vary with the number of included voxels, whereas the cluster-based analysis will not be as sensitive to this parameter. Finally, the inclusion in the tumor ROI of healthy tissue by the rater should be detected with the cluster-based analysis, i.e., the clustering should yield a cluster with the properties of a healthy tissue. This is not the case for the ROI-based analysis. In this case, the mean parameter value should be modified towards that of healthy tissue, thereby masking the contrast between tumor and healthy tissue.

In this preclinical study, we used quantitative parameters that are not routinely used in clinic. Further studies should be conducted on non-quantitative parameters, such as ratio between the parameter values measured in the tumor and in a normal appearing white matter area, as typically performed in clinical settings. Note that the cluster-based analysis could also help in selecting normal white appearing matter using the homogeneous MR characteristics intrinsic to this tissue.

In order to investigate the potential of the clustering approach for treatment follow up, we used the antiangiogenic-based vascular normalization hypothesis<sup>36</sup>, which was already validated in animal model studies<sup>21,13,25</sup>, followed by a radiotherapy. This study was not directly designed to investigate treatment efficacy and, although we observed an effect of Sora treatment, we could only detect minor effects of the combined therapy that could have been improved with a larger number of included animals.

The cluster-based approach may seem limited to follow-up spatial evolutions within the tumor when the tumor volume changes during progression and treatment. However, the cluster-based approach can potentially promote direct information of the short-term effect of treatment and/or about tumor with low progression rate such as low-grade glioma. Under these conditions, the cluster approach may help identify the tissue types that respond to a given therapy and may then be used to monitor dose response trials. For example, in our

study, a tumor with limited number of voxels belonging to cluster  $a$  and  $b$ , *i.e.* clusters responding to Sorafenib, will most probably show limited response under Sorafenib treatment. Overall, this strategy opens a new way to personalize therapy for each patient.

## **5. Conclusion**

In the context of combined therapies for solid tumor treatment, the cluster-based analysis and the ROI-based analysis provides complementary views of the same data. The ROI-based analysis is well suited to highlight global changes and the cluster-based analysis provides a comprehensive and subtle view of MRI-parameters integration that describes intra-tumoral heterogeneity. The evolution of the cluster distributions within the tumor appears as a promising strategy to decipher the complexity of tumor changes under combined therapies.

***Acknowledgments:***

We thank the animal care facility of GIN, the IRMaGe facility, the European Synchrotron factory, Elke Bräuer-Krisch for technical support and Bayer Bioscience for providing Sorafenib.

The authors also thank the “Conseil Régional Rhône-Alpes”, la “Ligue contre le Cancer, comité de la Drome”, “l’Association pour la Recherche contre le Cancer”, ANR-11-BSV5-004, and ANR-11-LABX-0063/ ANR-11-IDEX-0007 for their financial supports. Grenoble MRI facility IRMaGe was partly funded by the French program “Investissement d’Avenir” run by the “Agence Nationale pour la Recherche”; grant “Infrastructure d’avenir en Biologie Santé” - ANR-11-INBS-0006.

## References

1. Stupp R, Mason WP, van den Bent MJ, et al. Radiotherapy plus concomitant and adjuvant temozolomide for glioblastoma. *N Engl J Med*. 2005;352(10):987-996.
2. Tanaka S, Louis DN, Curry WT, Batchelor TT, Dietrich J. Diagnostic and therapeutic avenues for glioblastoma: no longer a dead end? *Nat Rev Clin Oncol*. 2013;10(1):14-26.
3. Chen J, Xu T. Recent therapeutic advances and insights of recurrent glioblastoma multiforme. *Front Biosci (Landmark Ed)*. 2013;18:676-684.
4. Hainsworth JD, Ervin T, Friedman E, et al. Concurrent radiotherapy and temozolomide followed by temozolomide and sorafenib in the first-line treatment of patients with glioblastoma multiforme. *Cancer*. 2010;116(15):3663-3669.
5. Den RB, Kamrava M, Sheng Z, et al. A Phase I Study of the Combination of Sorafenib With Temozolomide and Radiation Therapy for the Treatment of Primary and Recurrent High-Grade Gliomas. *International Journal of Radiation Oncology\*Biophysics\*Physics*. 2013;85(2):321-328.
6. Jain RK. Normalization of Tumor Vasculature: An Emerging Concept in Antiangiogenic Therapy. *Science*. 2005;307(5706):58-62.
7. Winkler F, Kozin SV, Tong RT, et al. Kinetics of vascular normalization by VEGFR2 blockade governs brain tumor response to radiation. *Cancer Cell*. 2004;6(6):553-563.
8. Barbier EL, Lamalle L, Décorps M. Methodology of brain perfusion imaging. *Journal of Magnetic Resonance Imaging*. 2001;13(4):496-520.
9. Troprès I, Grimault S, Vaeth A, et al. Vessel size imaging. *Magnetic Resonance in Medicine*. 2001;45(3):397-408.
10. He X, Yablonskiy DA. Quantitative BOLD: Mapping of human cerebral deoxygenated blood volume and oxygen extraction fraction: Default state. *Magnetic Resonance in Medicine*. 2007;57(1):115-126.
11. Tofts PS, Brix G, Buckley DL, et al. Estimating kinetic parameters from dynamic contrast-enhanced t1-weighted MRI of a diffusable tracer: Standardized quantities and symbols. *Journal of*

*Magnetic Resonance Imaging*. 1999;10(3):223–232.

12. Krainik A, Hund-Georgiadis M, Zysset S, Cramon DY von. Regional Impairment of Cerebrovascular Reactivity and BOLD Signal in Adults After Stroke. *Stroke*. 2005;36(6):1146-1152.
13. Lemasson B, Bouchet A, Maisin C, et al. Multiparametric MRI as an early biomarker of individual therapy effects during concomitant treatment of brain tumours. *NMR Biomed*. 2015;28(9):1163-1173.
14. Ken S, Deviers A, Filleron T, et al. Voxel-based evidence of perfusion normalization in glioblastoma patients included in a phase I–II trial of radiotherapy/tipifarnib combination. *J Neurooncol*. 2015;124(3):465-473.
15. Fraley C, Raftery AE. Model-Based Clustering, Discriminant Analysis, and Density Estimation. *Journal of the American Statistical Association*. 2002;97(458):611-631.
16. Coquery N, Francois O, Lemasson B, et al. Microvascular MRI and unsupervised clustering yields histology-resembling images in two rat models of glioma. *J Cereb Blood Flow Metab*. 2014;34(8):1354-1362.
17. Kilkenny C, Browne WJ, Cuthill IC, Emerson M, Altman DG. Improving Bioscience Research Reporting: The ARRIVE Guidelines for Reporting Animal Research. *PLOS Biology*. 2010;8(6):e1000412.
18. Coquery N, Pannetier N, Farion R, et al. Distribution and Radiosensitizing Effect of Cholesterol-Coupled Dbait Molecule in Rat Model of Glioblastoma. *PLoS ONE*. 2012;7(7):e40567.
19. Hirschler L, Debacker CS, Voiron J, Köhler S, Warnking JM, Barbier EL. Interpulse phase corrections for unbalanced pseudo-continuous arterial spin labeling at high magnetic field. *Magn Reson Med*. 2017;79(3):1314-1324.
20. Troprès I, Lamalle L, Péoc'h M, et al. In vivo assessment of tumoral angiogenesis. *Magn Reson Med*. 2004;51(3):533-541.
21. Lemasson B, Serduc R, Maisin C, et al. Monitoring Blood-Brain Barrier Status in a Rat Model of Glioma Receiving Therapy: Dual Injection of Low-Molecular-Weight and Macromolecular MR Contrast Media. *Radiology*. 2010;257(2):342-352.

22. Alsop DC, Detre JA. Reduced Transit-Time Sensitivity in Noninvasive Magnetic Resonance Imaging of Human Cerebral Blood Flow. *J Cereb Blood Flow Metab.* 1996;16(6):1236-1249.
23. Buxton RB, Frank LR, Wong EC, Siewert B, Warach S, Edelman RR. A general kinetic model for quantitative perfusion imaging with arterial spin labeling. *Magn Reson Med.* 1998;40(3):383-396.
24. Christen T, Lemasson B, Pannetier N, et al. Evaluation of a quantitative blood oxygenation level-dependent (qBOLD) approach to map local blood oxygen saturation. *NMR in Biomedicine.* 2011;24(4):393-403.
25. Lemasson B, Christen T, Tizon X, et al. Assessment of multiparametric MRI in a human glioma model to monitor cytotoxic and anti-angiogenic drug effects. *NMR in Biomedicine.* 2011;24(5):473-482.
26. Lemasson B, Christen T, Serduc R, et al. Evaluation of the Relationship between MR Estimates of Blood Oxygen Saturation and Hypoxia: Effect of an Antiangiogenic Treatment on a Gliosarcoma Model. *Radiology.* 2012;265(3):743-752.
27. Valable S, Lemasson B, Farion R, et al. Assessment of blood volume, vessel size, and the expression of angiogenic factors in two rat glioma models: a longitudinal in vivo and ex vivo study. *NMR Biomed.* 2008;21(10):1043-1056.
28. Lemasson B, Valable S, Farion R, Krainik A, Rémy C, Barbier EL. In vivo imaging of vessel diameter, size, and density: A comparative study between MRI and histology. *Magnetic Resonance in Medicine.* 2013;69(1):18–26.
29. Cha S. Neuroimaging in neuro-oncology. *Neurotherapeutics.* 2009;6(3):465-477.
30. Galbán CJ, Chenevert TL, Meyer CR, et al. The parametric response map is an imaging biomarker for early cancer treatment outcome. *Nat Med.* 2009;15(5):572-576.
31. Hamstra DA, Chenevert TL, Moffat BA, et al. Evaluation of the functional diffusion map as an early biomarker of time-to-progression and overall survival in high-grade glioma. *PNAS.* 2005;102(46):16759-16764.
32. Aronen HJ, Gazit IE, Louis DN, et al. Cerebral blood volume maps of gliomas: comparison with

tumor grade and histologic findings. *Radiology*. 1994;191(1):41-51.

33. Emblem KE, Nedregaard B, Nome T, et al. Glioma grading by using histogram analysis of blood volume heterogeneity from MR-derived cerebral blood volume maps. *Radiology*. 2008;247(3):808-817.

34. Chung C, Jalali S, Foltz W, et al. Imaging Biomarker Dynamics in an Intracranial Murine Glioma Study of Radiation and Antiangiogenic Therapy. *International Journal of Radiation Oncology\*Biological\*Physics*. 2013;85(3):805-812.

35. Hamstra DA, Rehemtulla A, Ross BD. Diffusion Magnetic Resonance Imaging: A Biomarker for Treatment Response in Oncology. *JCO*. 2007;25(26):4104-4109.

36. Goel S, Duda DG, Xu L, et al. Normalization of the Vasculature for Treatment of Cancer and Other Diseases. *Physiological Reviews*. 2011;91(3):1071-1121.

## Figure Legends

**Figure 1. A. Experimental design.** At D0, rats were implanted with F98 glioblastoma cells (as mentioned above). Twenty day after cell inoculation (D20), a control MRI session was performed. One day later (D21) Sorafenib (Sora: 30 mg/kg) or vehicle was administrated during three day, one administration p.o. per day (D21T0 to D23T3). Then, at D24T3, a second MRI session was performed in the morning and some rats underwent a radiotherapy (20Gy) in the afternoon. Two days after irradiation (D26T5), a third MRI session was performed. D as notation for the duration (days) after tumor cell implantation, and T as the duration (days) after treatment initiation. **B. Experimental groups.** At D20T-1, before treatment: group C. At D24T3, after vehicle administration: group V; or after Sorafenib administration: group S. At D25T5, vehicle administration followed by irradiation: group VRT; Sorafenib treatment followed by irradiation: group SRT; Sorafenib treatment followed by no irradiation: group SØ. Animal numbers are presented for each group.

**Figure 2. Multiparametric MRI of F98 glioma under Sorafenib treatment, radiotherapy and combined treatments.** (A) In addition to anatomical T<sub>2</sub>W images, six MRI parameters were mapped: ADC, Perm, CBF, CBV, VSI and StO<sub>2</sub>. The tumor ROIs are overlaid on the maps. (B) Representative view of the ROI-based analysis from baseline at D20T-1. (C) Mean ± SEM of tumor ADC, Perm, CBF, CBV, VSI and StO<sub>2</sub> at different time points of group: C (before treatment); V: after vehicle administration; S: after Sorafenib administration; VRT: vehicle administration followed by irradiation; SRT: Sorafenib treatment followed by irradiation and SØ: Sorafenib treatment followed by no irradiation. Comparison between D20T-1 and D24T3: RM-ANOVA, \* p<0.05 for the effect of Sorafenib treatment. Comparison between D24T3 and D26T5: RM-ANOVA with LSD post-hoc correction for

multiple comparisons: \*  $p < 0.05$  for VRT vs SRT, \$  $p < 0.05$  for VRT vs SØ. **(D)** Tumor size progression. Mean  $\pm$  SD. Baseline D20T-1 (C, n=19), D24T3 (V, n=7; S n=12), D26T5 (VRT, n=7; SRT, n=7; SØ, n=5)

**Figure 3. Cluster distribution and characterization.** **(A)** Cluster characterization with web graph representing the mean standardized value and mean  $\pm$  SEM values for each MRI parameter. **(B)** Cluster assignment within tumor ROI overlaid on the T<sub>2</sub>W anatomical image. The coloured bars show the cluster proportion within the ROI for each condition (time points and treatments). Baseline D20T-1 (C, n=17), D24T3 (V, n=5; S, n=12), D26T5 (VRT, n=5; SRT, n=7; SØ, n=5), np : non physiological values.

**Figure 4. ROI-based and Cluster-based changes following therapy.** For each time interval, MRI parameter evolutions, a representative map of cluster distribution, and the evolution of the percentage of each cluster (*a* to *e*) are presented. This highlights the impact of treatments independently of tumor characteristics before treatment. **(A)** Changes between D20T-1 and D24T3 **(B)**. Changes between D24T3 and D26T5. Mean  $\pm$  SEM. Mann-Whitney test, \*  $p < 0.05$

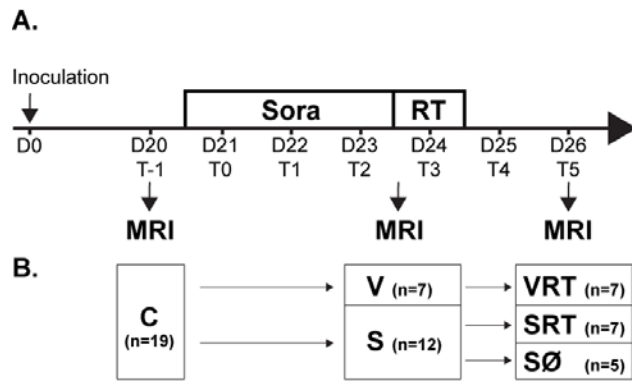


**Figure 1**

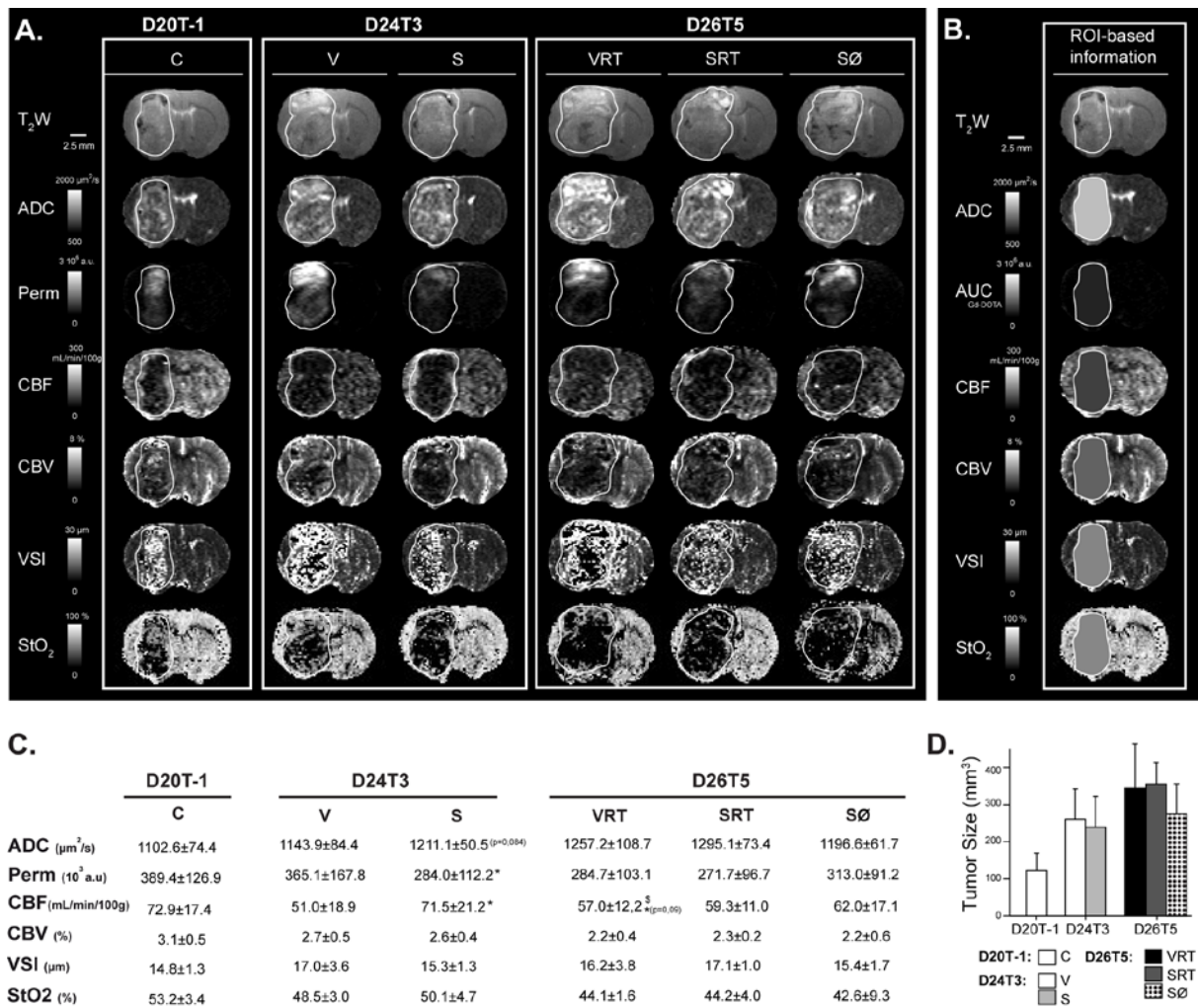


**Figure 2**

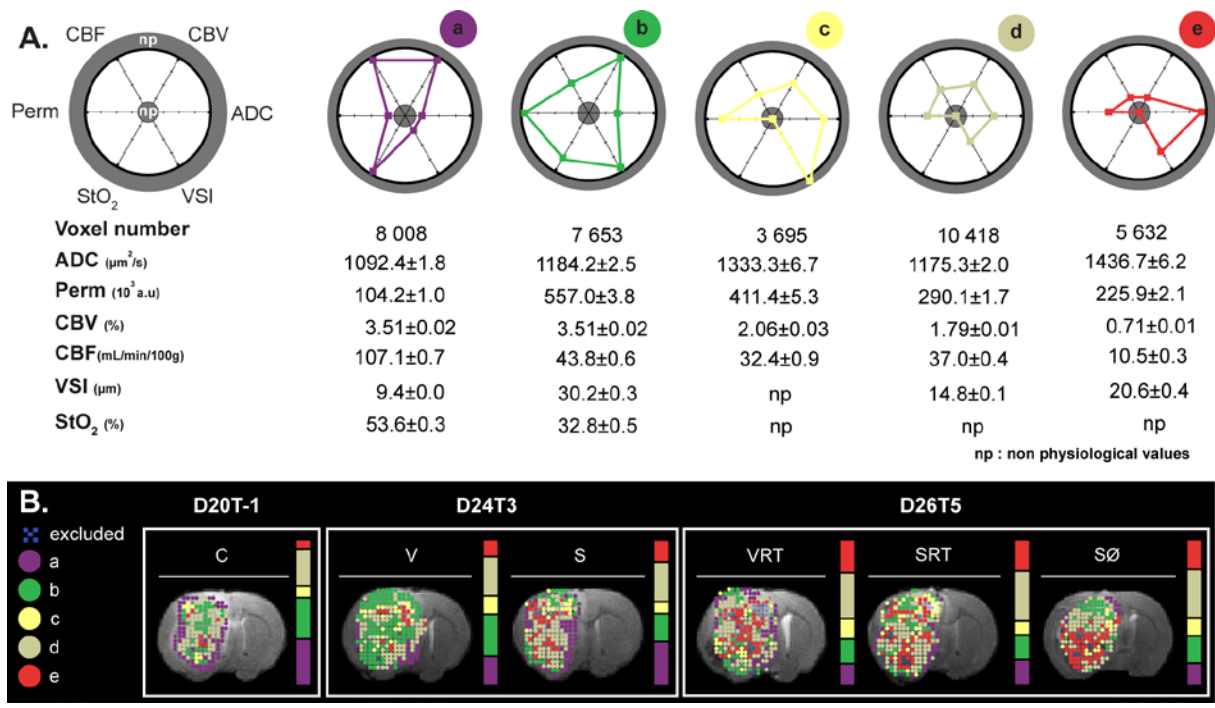


**Figure 3**

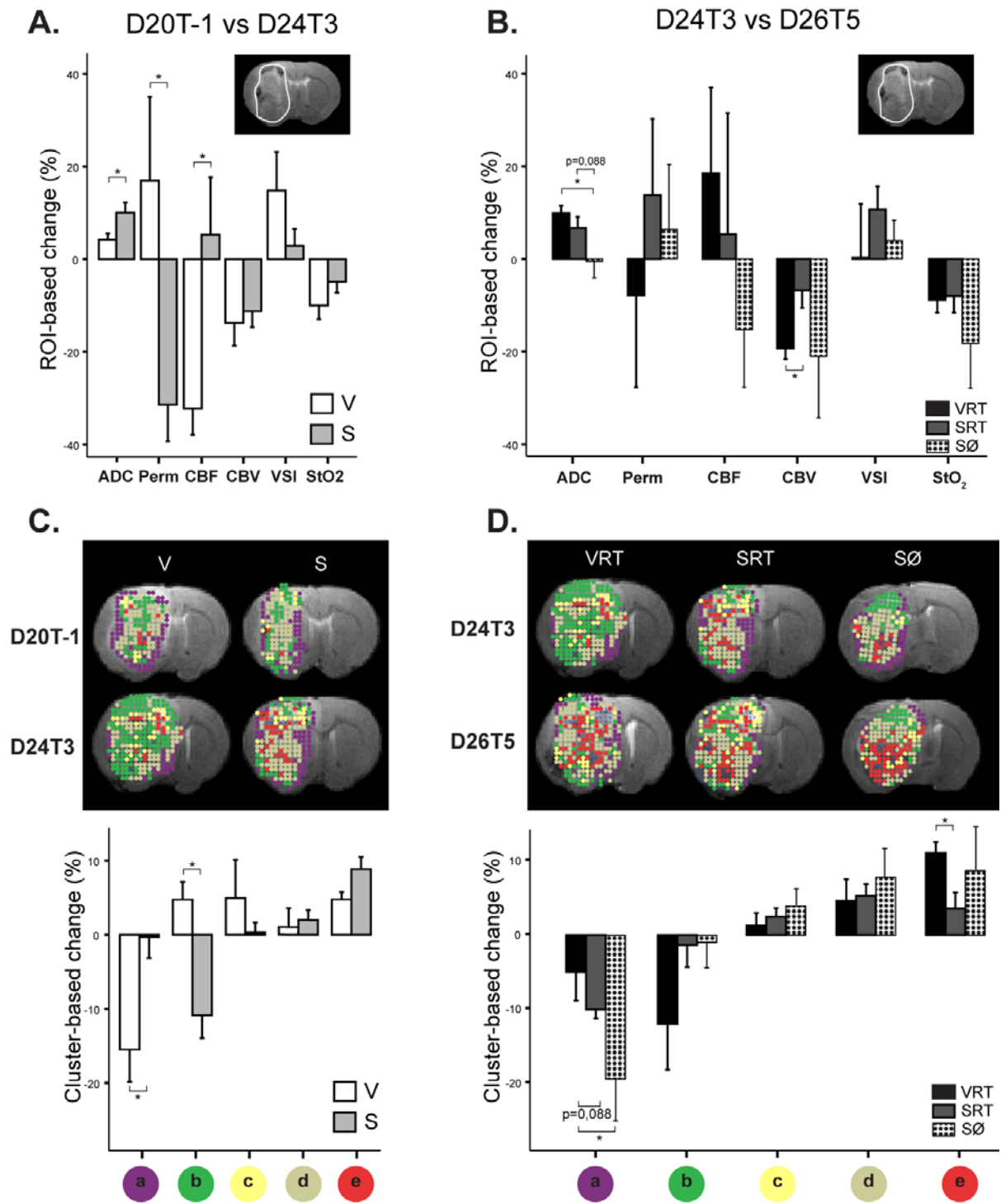


**Figure 4**